

**Supporting information**

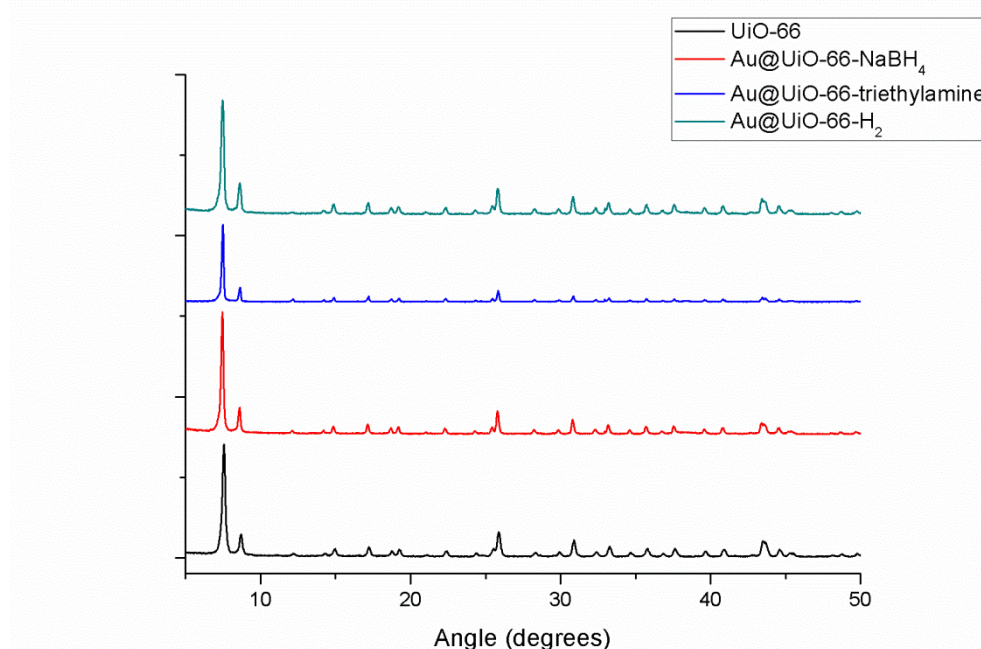


Fig S.1 XRPD patterns of the UiO-66 and Au@UiO-66 materials.

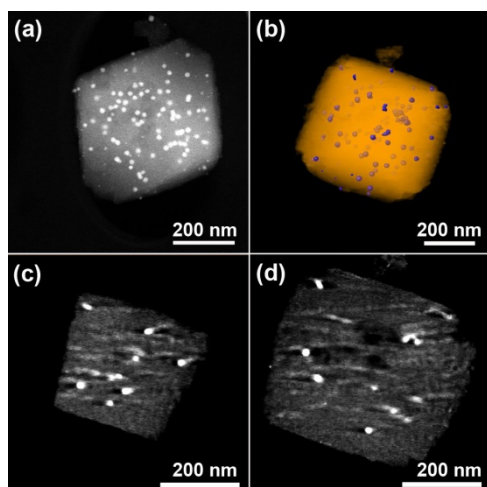


Fig S.2 . HAADF-STEM electron tomography reconstruction of the Au@UiO-66-H<sub>2</sub> material. (a) HAADF-STEM image of the Au-loaded UiO-66 crystal used for tomographic reconstruction. (b) Reconstructed volume, with the UiO-66 matrix rendered in Orange, and the Au nanoparticles in Blue. (c)&(d) Orthoslices through the reconstructed volume, evidencing that the bright-contrast Au nanoparticles are spread throughout the UiO-66 matrix.

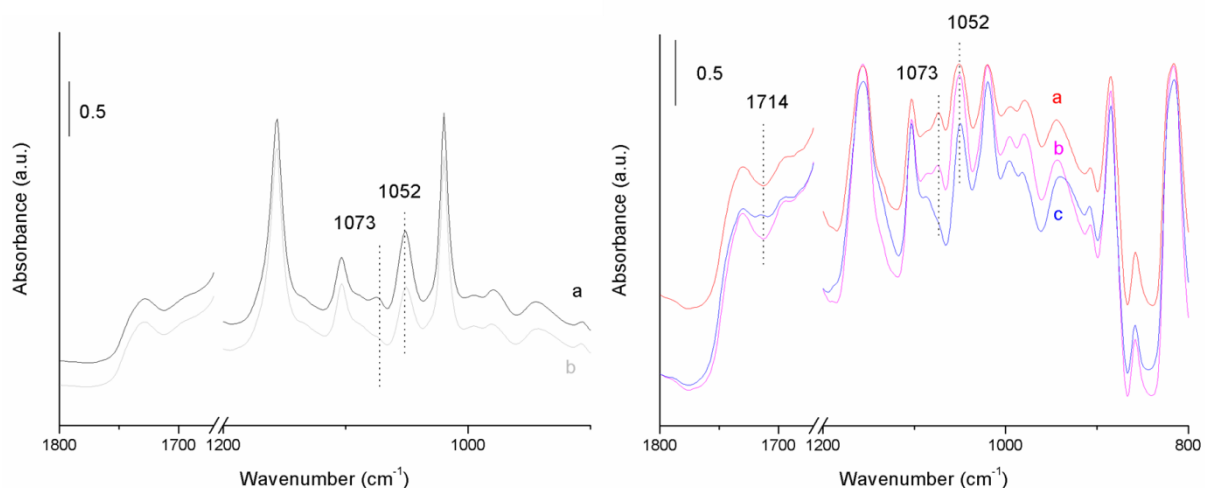
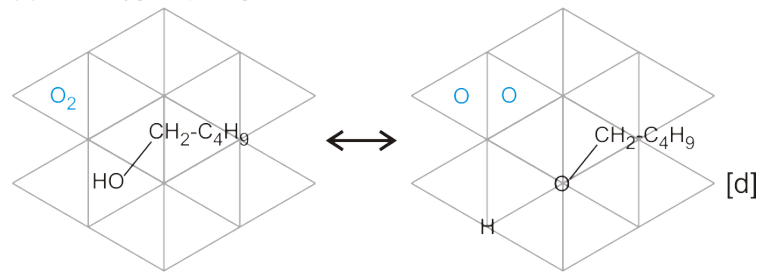
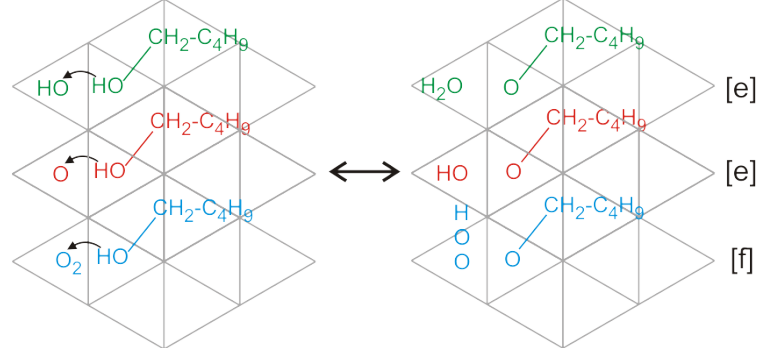


Fig S.3 Left: IR spectra of pentanol (3mbar) adsorbed on the Au@UiO-66-NaBH<sub>4</sub> sample in the absence of O<sub>2</sub> at 25°C (a) and 60°C (b). Right: IR spectra of pentanol (3mbar) adsorbed on the Au@UiO-66-NaBH<sub>4</sub> sample in the presence of 15mbar O<sub>2</sub> at 25°C (a), 60°C (b) and 100°C (c).

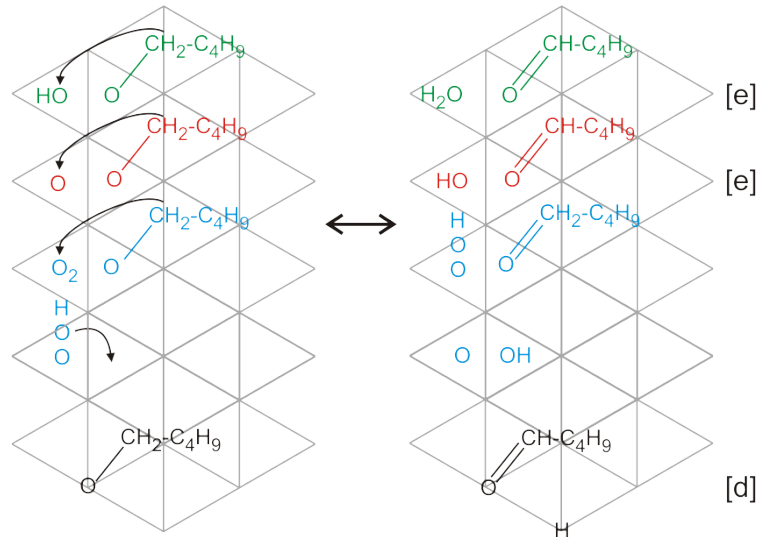
(a) initial oxygen splitting and alkoxide formation



(b) alkoxide formation via deprotonation on hydroxyl, oxo or peroxy species



(c) aldehyde formation via deprotonation on hydroxyl, oxo or peroxy species



Scheme S. 1. Plausible oxidation mechanism on the Au Nanoparticles, schematically shown on a Au(111) surface. The symbols refer to articles where similar reaction pathways are postulated: [d]<sup>1</sup>, [e]<sup>2</sup> and [f]<sup>3</sup>.

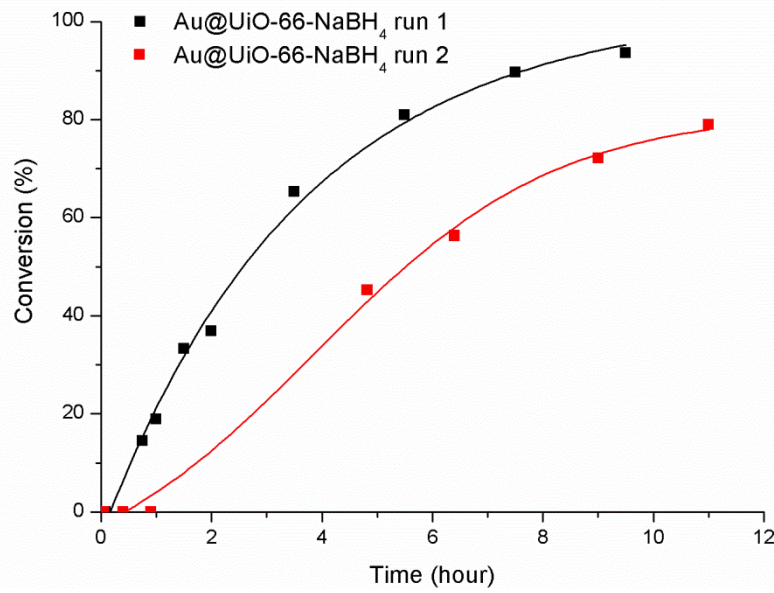


Fig S.4 Benzyl alcohol conversion in the first and second run using Au@UiO-66-NaBH<sub>4</sub> as catalyst

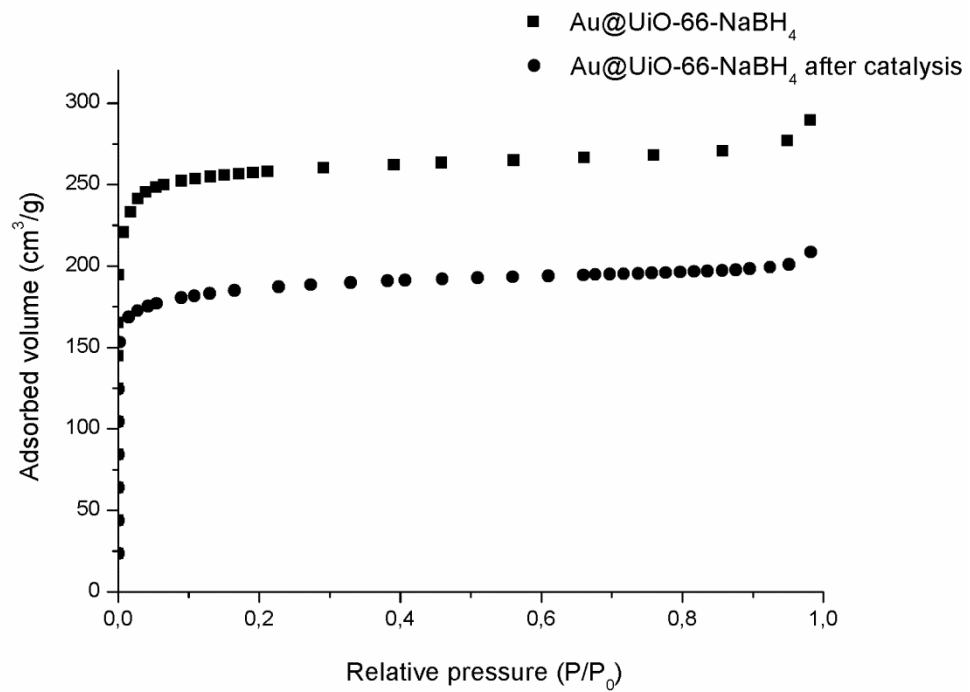
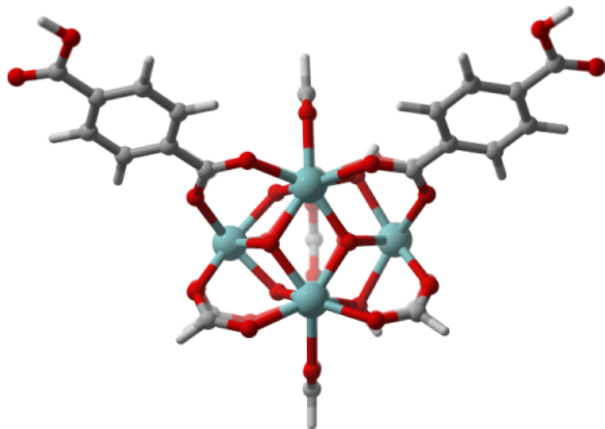


Fig S.5 N<sub>2</sub> sorption isotherm of Au@UiO-66-NaBH<sub>4</sub> before (■) and after catalysis (●)

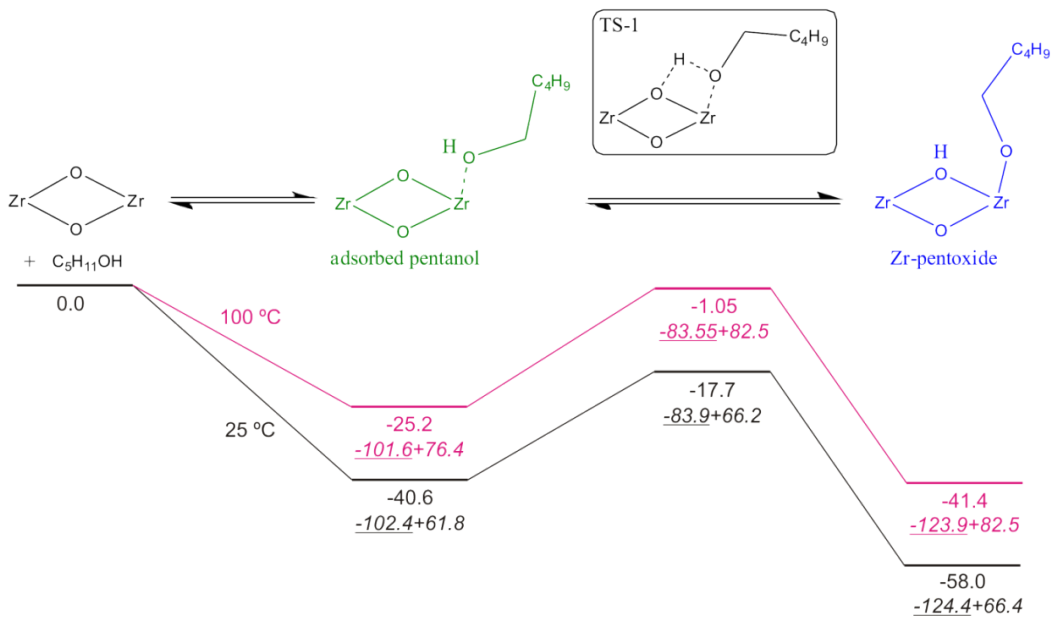
## Cluster calculations

The cluster model used in this paper is the same as applied earlier in the paper of Vermoortele et al.<sup>4</sup> (**Figure S.6**). Geometry optimizations were performed with the Gaussian09 package<sup>5</sup> using the B3LYP hybrid functional.<sup>6</sup> The double-zeta Pople basis set 6-31g(d) was used for all atoms except for Zr, for which the LANL2DZ effective core potential and basis set were applied.<sup>7</sup> Afterwards single point energy refinements at the B3LYP/6-311++g(d,p) level of theory were performed to account for the electronic energy effects of the substituents on the terephthalate linkers, employing the LANL2TZ(f) effective core potential and basis set for Zr<sup>8</sup>. Furthermore, van der Waals corrections of the type D3 as developed by Grimme<sup>9</sup> in conjunction with the B3LYP functional were computed. Using the standard notation “LOT-E”//“LOT-G” (LOT-E and LOT-G being the electronic levels of theory used for the energy and geometry optimizations, respectively), all cluster results discussed in this paper are obtained with the method denoted as “B3LYP/6-311++g(d,p)\*-D3//B3LYP/6-31g(d)\*”. The PHVA method<sup>10</sup>, applied also previously for kinetics<sup>4, 11</sup>, was then used to investigate the kinetics of the pentoxide formation on the extended UiO-66 cluster.



**Fig S.6** Extended cluster model for UiO-66. The terephthalic linkers closest to the considered active site are maintained.

Accessible Zr-sites form strong Lewis acid adsorption sites, and experimentally, after loading of pentanol an equilibrium between gas phase and adsorbed pentanol will be installed. Pentanol can either be physisorbed or chemisorbed on the Zr-defect sites within the UiO-66 (Scheme S.2). A free energy profile was determined based on the extended UiO-66 cluster model, as displayed in Figure S.9.<sup>4</sup> Gibbs free energy differences are reported in Scheme S.2, as well as the enthalpy and entropy contributions. At 25 °C, the adsorption free energy of a linearly adsorbed pentanol is -40.6 kJ/mol but this decreases with increasing temperature due to a large entropic penalty. Furthermore, the pentoxide formation from (linearly) adsorbed pentanol is both exergonic and exothermic, and only a small free energy barrier needs to be overcome, which probably can even decrease when the environment is fully taken into account.



Scheme S.2. Equilibrium between gas phase pentanol, adsorbed pentanol (physisorption) and Zr-pentoxide (chemisorption). Free energy profile at 25 °C (black) and at 100 °C (red) with a pentanol pressure of 3mbar. Enthalpy and entropy contributions to the free energies are also given in kJ/mol. Extended cluster (Fig. S.6) results at B3LYP/6-311++g(d,p)\*-D3//B3LYP/6-31g(d)\*.

## Molecular dynamics simulations

### Construction of the models

We performed calculations on a fully periodic UiO-66 model with unit cell formula  $[\text{Zr}_6\text{O}_5(\text{OH})_2(\text{RCOO})_{10}][\text{Zr}_6\text{O}_4(\text{OH})_4(\text{RCOO})_{12}]$  (one BDC linker consists of two RCOO units). The structure exhibits one missing BDC linker, which leads to a topology with straight parallelogram shaped channels throughout the material (**Fig S.7**, pore size  $\sim 10$ - $11$  Å). The unit cell was then optimized with the Vienna Ab Initio Simulation Package (VASP 5.2.12)<sup>12</sup>. We applied a plane wave kinetic energy cutoff of 600 eV, employing the PBE exchange-correlation functional<sup>13</sup> with D3-dispersion corrections including Becke-Johnson damping<sup>14</sup>. Subsequently, we ran molecular dynamics simulations starting from two different placements of pentanol (adsorbed pentanol and chemisorbed pentanol or Zr-pentoxide).

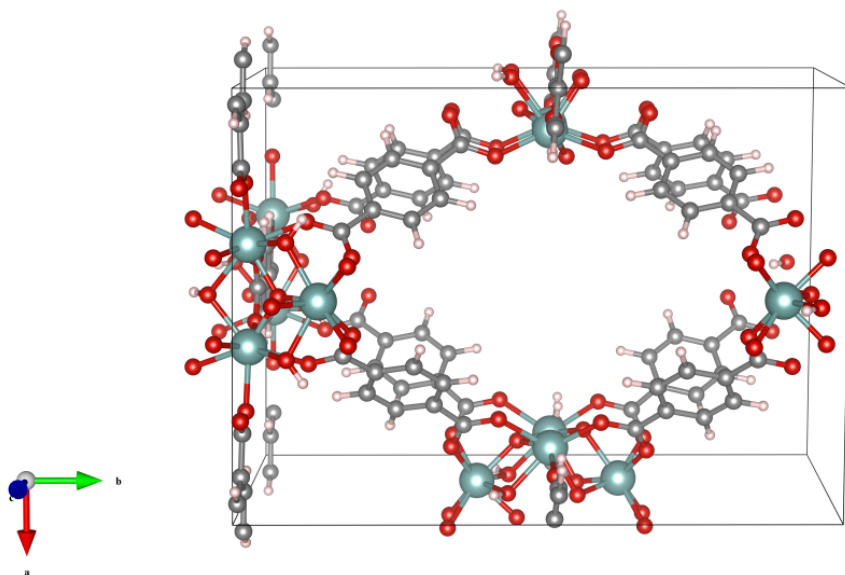


**Fig S.7** Applied periodic model for the UiO-66 with one missing linker.

Au nanoparticles were generated using the program OpenMD ([www.openmd.org](http://www.openmd.org)) applying the Sutton-Chen formulation of the Finnis-Sinclair metallic potential using quantum corrections according to Kimura et al<sup>15</sup>. We generated a NP of 55 atoms,<sup>16</sup> and removed one atom to obtain a NP of 54 atoms. Having an even number of Au-atoms makes it possible to model the system without spin polarization, an approach that is frequently used when Au-NP are considered<sup>2</sup>. Similar to the UiO-66 case, adsorbed and chemisorbed states of pentanol were constructed for further investigation by molecular dynamics simulations.

### Computational Methodology

AIMD simulations were performed with the CP2K simulation package<sup>17</sup> on the DFT level of theory and with Gaussian Plane Wave basis sets (GPW)<sup>18</sup>. The BLYP functional<sup>19</sup> was chosen including Grimme D3 dispersion corrections<sup>14a</sup>. The DZVP-GTH basis set<sup>20</sup> was applied for all atoms except for Zr and Au, in which we opted for the MOLOPT-DZVP-GTH basis set<sup>21</sup>. The time step for integration of the equations of motion was set to 0.5 fs. The simulations were performed within the NVT ensemble (P=1bar, T=298K). The

velocities are updated each time step during the *ab initio* molecular dynamics run (see computational details in the Supporting Information). The Velocity Power Spectrum (VPS) was generated with MD-tracks.<sup>22</sup> The analysis was performed on 126000 MD-steps of 1 fs, starting from an equilibrated structure (obtained after an initial MD run of 1 ps). The input velocities were divided in 12 blocks and subsequently a Fourier transform of each block was calculated and the final VPS was constructed from the average over all the blocks. Remark that a larger number of blocks leads to an improved statistical accuracy of the amplitudes, however, a reduced resolution of the frequency scale.<sup>23</sup>

Furthermore, the wavenumbers were scaled (scaling factor = 0.98) to obtain a good comparison with experimental data. An overview of all VPS spectra plotted together is given in **Fig. S.8**, while the standard deviation on the amplitudes is given in **Figures S.9-S.12**.

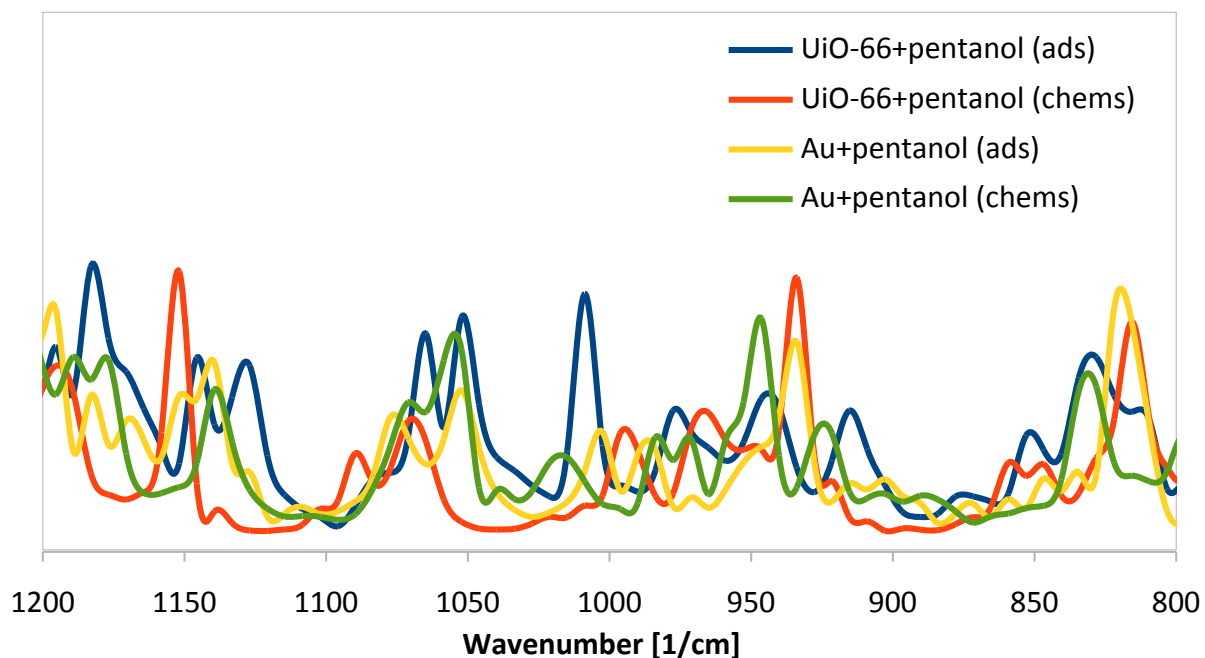


**Fig S.8** Smoothed velocity power spectra of pentanol for the 4 systems that were used.

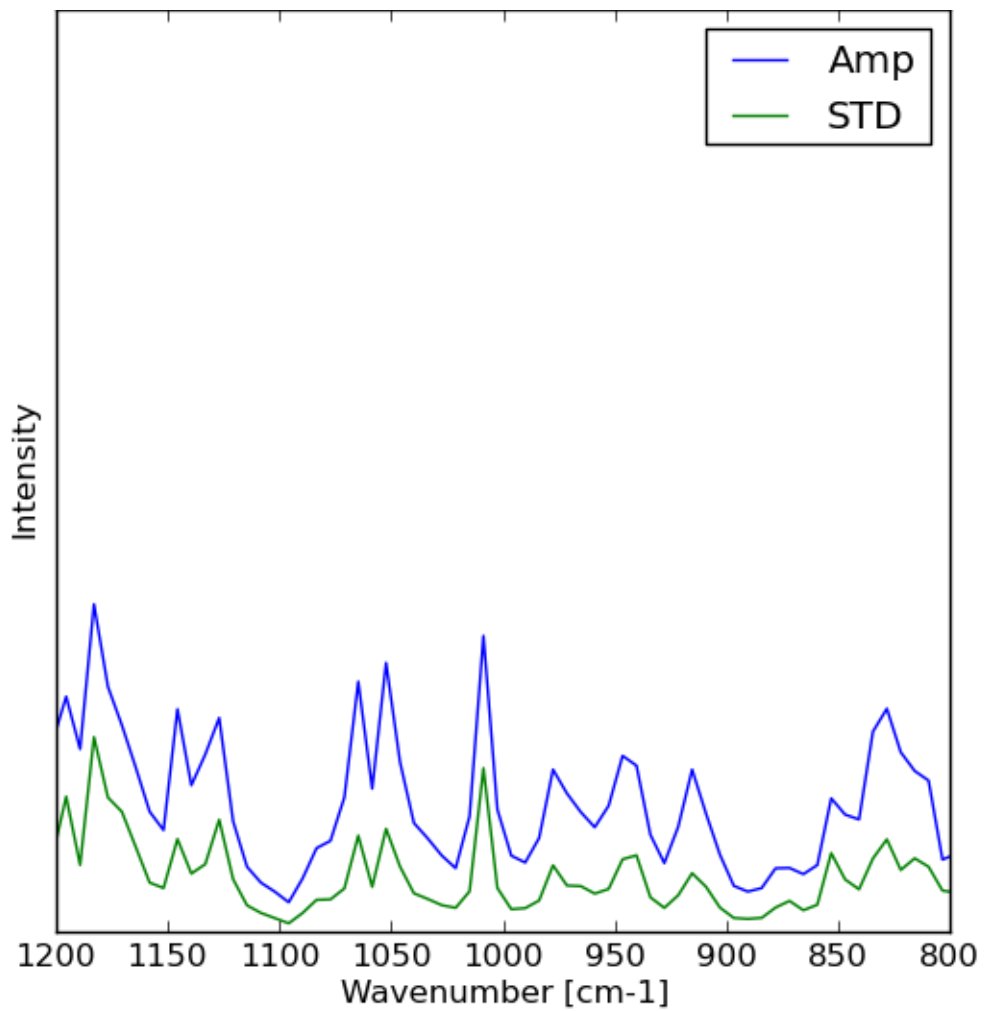


**Fig S.9** Velocity power spectra of pentanol for the UiO-66 model with adsorbed pentanol.<sup>23</sup>

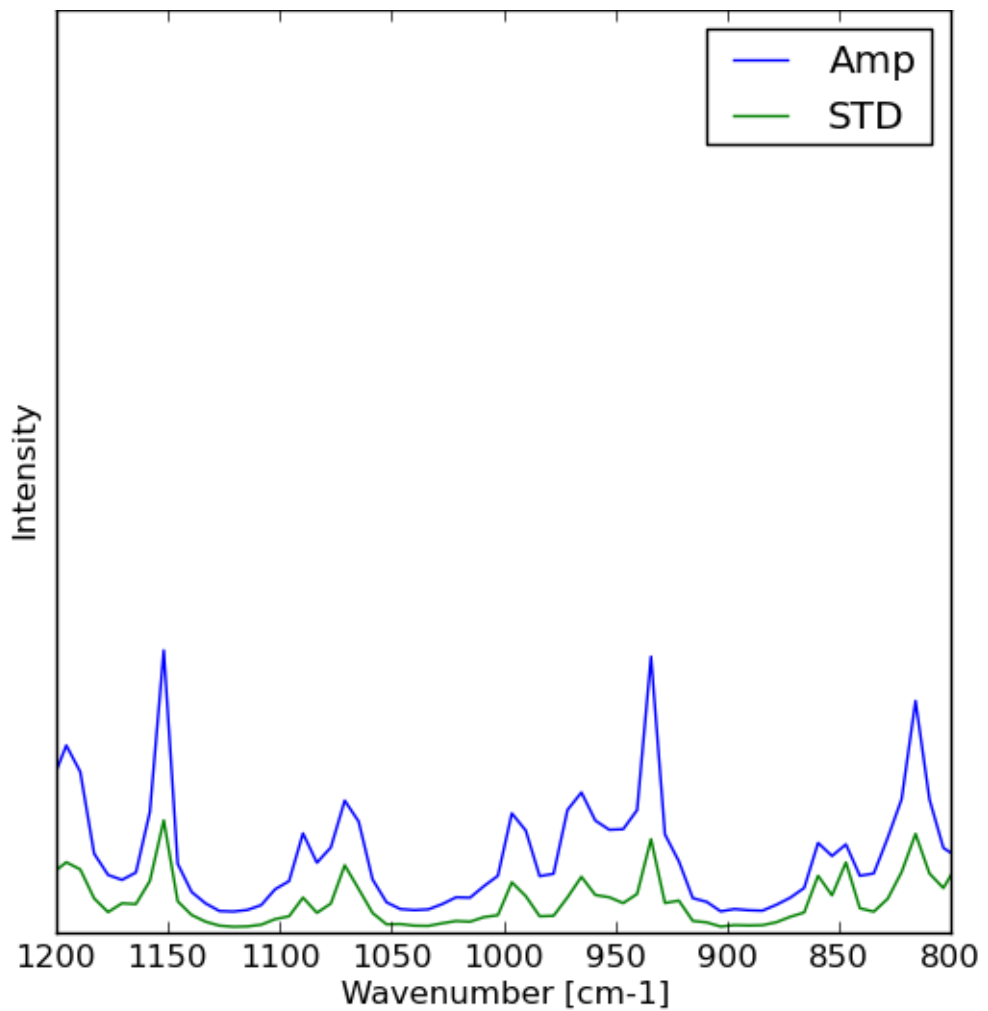


**Fig S.10** Velocity power spectra of pentanol for the UiO-66 model with chemisorbed pentanol.<sup>23</sup>

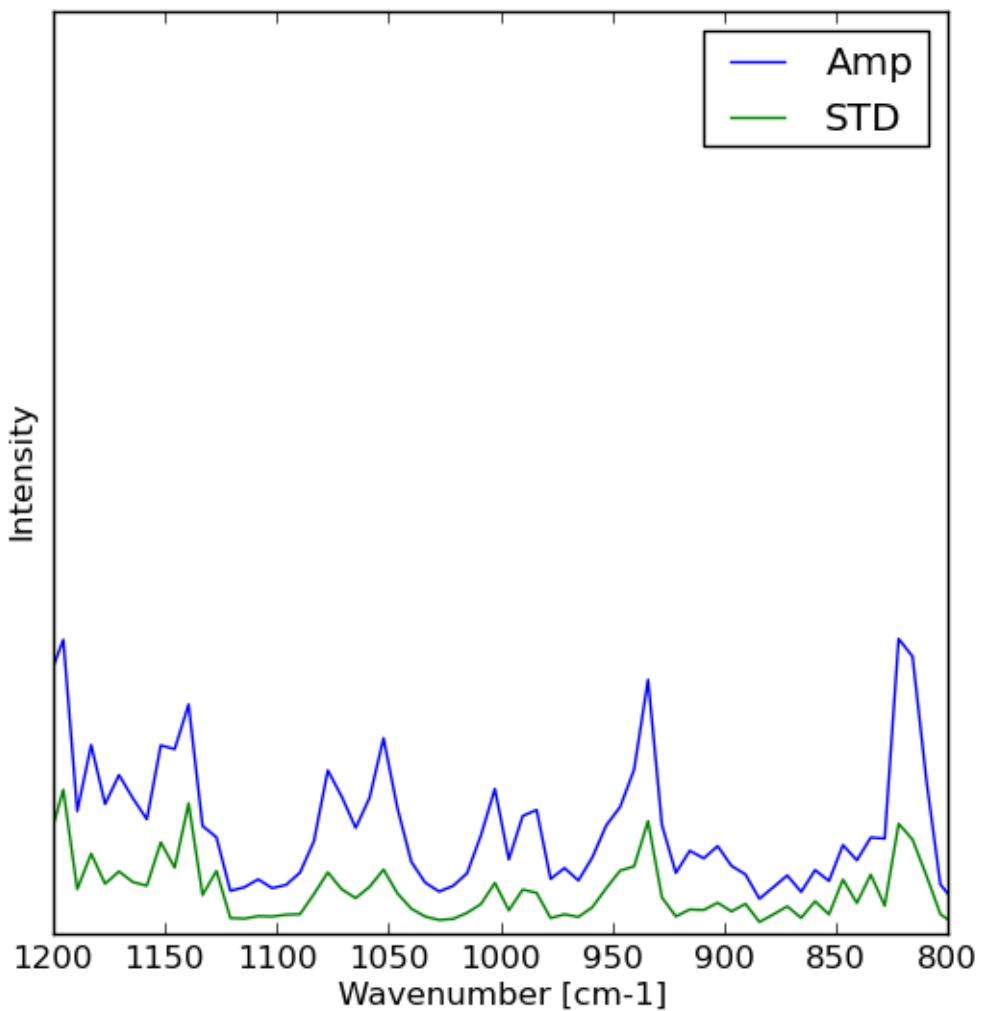


**Fig S.11** Velocity power spectra of pentanol for the Au model with adsorbed pentanol.<sup>23</sup>

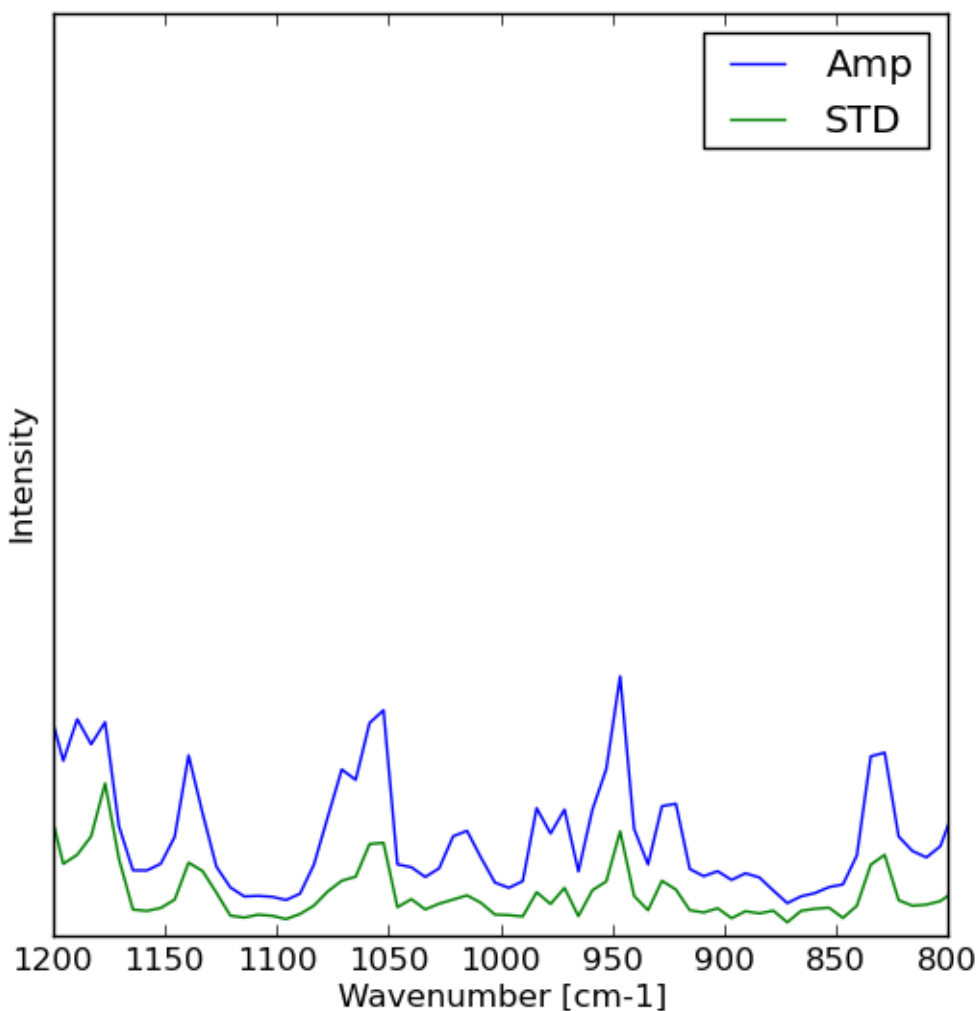


**Fig S.12** Velocity power spectra of pentanol for the Au model with chemisorbed pentanol.<sup>23</sup>

## References

1. Mullen, G. M.; Zhang, L.; Evans, E. J.; Yan, T.; Henkelman, G.; Mullins, C. B., Oxygen and Hydroxyl Species Induce Multiple Reaction Pathways for the Partial Oxidation of Allyl Alcohol on Gold. *Journal of the American Chemical Society* **2014**, *136* (17), 6489-6498.
2. Boronat, M.; Corma, A.; Illas, F.; Radilla, J.; Rodenas, T.; Sabater, M. J., Mechanism of selective alcohol oxidation to aldehydes on gold catalysts: Influence of surface roughness on reactivity. *J Catal* **2011**, *278* (1), 50-58.
3. Liu, H. L.; Liu, Y. L.; Li, Y. W.; Tang, Z. Y.; Jiang, H. F., Metal-Organic Framework Supported Gold Nanoparticles as a Highly Active Heterogeneous Catalyst for Aerobic Oxidation of Alcohols. *J Phys Chem C* **2010**, *114* (31), 13362-13369.
4. Vermoortele, F.; Vandichel, M.; Van de Voorde, B.; Ameloot, R.; Waroquier, M.; Van Speybroeck, V.; De Vos, D. E., Electronic Effects of Linker Substitution on Lewis Acid Catalysis with Metal-Organic Frameworks. *Angew Chem Int Edit* **2012**, *51* (20), 4887-4890.
5. Frisch, M. J. T., G. W.; Schlegel, H. B.; Scuseria, G. E.; Robb, M. A.; Cheeseman, J. R.; Scalmani, G.; Barone, V.; Mennucci, B.; Petersson, G. A.; Nakatsuji, H.; Caricato, M.; Li, X.; Hratchian, H. P.; Izmaylov, A. F.; Bloino, J.; Zheng, G.; Sonnenberg, J. L.; Hada, M.;

Ehara, M.; Toyota, K.; Fukuda, R.; Hasegawa, J.; Ishida, M.; Nakajima, T.; Honda, Y.; Kitao, O.; Nakai, H.; Vreven, T.; Montgomery, Jr., J. A.; Peralta, J. E.; Ogliaro, F.; Bearpark, M.; Heyd, J. J.; Brothers, E.; Kudin, K. N.; Staroverov, V. N.; Kobayashi, R.; Normand, J.; Raghavachari, K.; Rendell, A.; Burant, J. C.; Iyengar, S. S.; Tomasi, J.; Cossi, M.; Rega, N.; Millam, N. J.; Klene, M.; Knox, J. E.; Cross, J. B.; Bakken, V.; Adamo, C.; Jaramillo, J.; Gomperts, R.; Stratmann, R. E.; Yazyev, O.; Austin, A. J.; Cammi, R.; Pomelli, C.; Ochterski, J. W.; Martin, R. L.; Morokuma, K.; Zakrzewski, V. G.; Voth, G. A.; Salvador, P.; Dannenberg, J. J.; Dapprich, S.; Daniels, A. D.; Farkas, O.; Foresman, J. B.; Ortiz, J. V.; Cioslowski, J.; Fox, D. J. *Gaussian 09, Revision A.02*, Gaussian, Inc., Wallingford CT: 2009.

6. (a) Becke, A. D., DENSITY-FUNCTIONAL THERMOCHEMISTRY .3. THE ROLE OF EXACT EXCHANGE. *Journal of Chemical Physics* **1993**, *98* (7), 5648-5652; (b) Lee, C. T.; Yang, W. T.; Parr, R. G., DEVELOPMENT OF THE COLLE-SALVETTI CORRELATION-ENERGY FORMULA INTO A FUNCTIONAL OF THE ELECTRON-DENSITY. *Physical Review B* **1988**, *37* (2), 785-789.
7. (a) Hay, P. J.; Wadt, W. R., Ab initio Effective Core Potentials for Molecular Calculations - Potentials for K to Au Including the Outermost Core Orbitals. *Journal of Chemical Physics* **1985**, *82* (1), 299-310; (b) Hay, P. J.; Wadt, W. R., Ab initio Effective Core Potentials for Molecular Calculations - Potentials for the Transition-Metal Atoms Sc to Hg. *Journal of Chemical Physics* **1985**, *82* (1), 270-283.
8. Roy, L. E.; Hay, P. J.; Martin, R. L., Revised basis sets for the LANL effective core potentials. *J Chem Theory Comput* **2008**, *4* (7), 1029-1031.
9. Grimme, S.; Antony, J.; Ehrlich, S.; Krieg, H., A consistent and accurate ab initio parametrization of density functional dispersion correction (DFT-D) for the 94 elements H-Pu. *Journal of Chemical Physics* **2010**, *132* (15), 154104.
10. (a) Ghysels, A.; Van Neck, D.; Waroquier, M., Cartesian formulation of the mobile block Hessian approach to vibrational analysis in partially optimized systems. *Journal of Chemical Physics* **2007**, *127*, 164108; (b) Ghysels, A.; Van Speybroeck, V.; Verstraelen, T.; Van Neck, D.; Waroquier, M., Calculating reaction rates with partial Hessians: Validation of the mobile block Hessian approach. *J Chem Theory Comput* **2008**, *4* (4), 614-625; (c) Ghysels, A.; Van Speybroeck, V.; Pauwels, E.; Van Neck, D.; Brooks, B. R.; Waroquier, M., Mobile Block Hessian Approach with Adjoined Blocks: An Efficient Approach for the Calculation of Frequencies in Macromolecules. *J Chem Theory Comput* **2009**, *5* (5), 1203-1215.
11. (a) Vandichel, M.; Lesthaeghe, D.; Van der Mynsbrugge, J.; Waroquier, M.; Van Speybroeck, V., Assembly of cyclic hydrocarbons from ethene and propene in acid zeolite catalysis to produce active catalytic sites for MTO conversion. *J Catal* **2010**, *271* (1), 67-78; (b) Vandichel, M.; Biswas, S.; Leus, K.; Paier, J.; Sauer, J.; Verstraelen, T.; Van der Voort, P.; Waroquier, M.; Van Speybroeck, V., Catalytic Performance of Vanadium MIL-47 and Linker-Substituted Variants in the Oxidation of Cyclohexene: A Combined Theoretical and Experimental Approach. *Chempluschem* **2014**, *79* (8), 1183-1197; (c) Vandichel, M.; Vermoortele, F.; Cottenie, S.; De Vos, D. E.; Waroquier, M.; Van Speybroeck, V., Insight in the activity and diastereoselectivity of various Lewis acid catalysts for the citronellal cyclization. *J Catal* **2013**, *305*, 118-129; (d) Vandichel, M.; Leus, K.; Van der Voort, P.; Waroquier, M.; Van Speybroeck, V., Mechanistic insight into the cyclohexene epoxidation with VO(acac)(2) and tert-butyl hydroperoxide. *J Catal* **2012**, *294*, 1-18; (e) Leus, K.; Vandichel, M.; Liu, Y. Y.; Muylaert, I.; Musschoot, J.; Pyl, S.; Vrielinck, H.; Callens, F.; Marin, G. B.; Detavernier, C.; Wiper, P. V.; Khimyak, Y. Z.; Waroquier, M.; Van Speybroeck, V.; Van der Voort, P., The coordinatively saturated vanadium MIL-47 as a low leaching heterogeneous catalyst in the oxidation of cyclohexene. *J Catal* **2012**, *285* (1), 196-

- 207; (f) Van Speybroeck, V.; Van der Mynsbrugge, J.; Vandichel, M.; Hemelsoet, K.; Lesthaeghe, D.; Ghysels, A.; Marin, G. B.; Waroquier, M., First Principle Kinetic Studies of Zeolite-Catalyzed Methylation Reactions. *Journal of the American Chemical Society* **2011**, *133* (4), 888-899; (g) Lesthaeghe, D.; Van der Mynsbrugge, J.; Vandichel, M.; Waroquier, M.; Van Speybroeck, V., Full Theoretical Cycle for both Ethene and Propene Formation during Methanol-to-Olefin Conversion in H-ZSM-5. *Chemcatchem* **2011**, *3* (1), 208-212.
12. (a) Kresse, G.; Furthmuller, J., Efficient iterative schemes for ab initio total-energy calculations using a plane-wave basis set. *Physical Review B* **1996**, *54* (16), 11169; (b) Kresse, G.; Furthmuller, J., Efficiency of ab-initio total energy calculations for metals and semiconductors using a plane-wave basis set. *Computational Materials Science* **1996**, *6* (1), 15-50; (c) Kresse, G.; Hafner, J., Ab initio molecular dynamics for liquid metals. *Physical Review B* **1993**, *47* (1), 558; (d) Kresse, G.; Hafner, J., Ab initio molecular-dynamics simulation of the liquid-metal-amorphous-semiconductor transition in germanium. *Physical Review B* **1994**, *49* (20), 14251.
13. (a) Perdew, J. P.; Burke, K.; Ernzerhof, M., Generalized Gradient Approximation Made Simple. *Physical Review Letters* **1996**, *77* (18), 3865; (b) Perdew, J. P.; Burke, K.; Ernzerhof, M., Generalized Gradient Approximation Made Simple [Phys. Rev. Lett. **77**, 3865 (1996)]. *Physical Review Letters* **1997**, *78* (7), 1396.
14. (a) Grimme, S.; Antony, J.; Ehrlich, S.; Krieg, H., A consistent and accurate ab initio parametrization of density functional dispersion correction (DFT-D) for the 94 elements H-Pu. *J Chem Phys* **2010**, *132* (15); (b) Grimme, S.; Ehrlich, S.; Goerigk, L., Effect of the Damping Function in Dispersion Corrected Density Functional Theory. *J Comput Chem* **2011**, *32* (7), 1456-1465.
15. Qi, Y.; Cagin, T.; Kimura, Y.; Goddard, W. A., Molecular-dynamics simulations of glass formation and crystallization in binary liquid metals: Cu-Ag and Cu-Ni. *Physical Review B* **1999**, *59* (5), 3527-3533.
16. Kleis, J.; Greeley, J.; Romero, N. A.; Morozov, V. A.; Falsig, H.; Larsen, A. H.; Lu, J.; Mortensen, J. J.; Dulak, M.; Thygesen, K. S.; Norskov, J. K.; Jacobsen, K. W., Finite Size Effects in Chemical Bonding: From Small Clusters to Solids. *Catal Lett* **2011**, *141* (8), 1067-1071.
17. VandeVondele, J.; Krack, M.; Mohamed, F.; Parrinello, M.; Chassaing, T.; Hutter, J., QUICKSTEP: Fast and accurate density functional calculations using a mixed Gaussian and plane waves approach. *Comput. Phys. Commun.* **2005**, *167* (2), 103-128.
18. (a) Lippert, G.; Hutter, J.; Parrinello, M., The Gaussian and augmented-plane-wave density functional method for ab initio molecular dynamics simulations. *Theor. Chem. Acc.* **1999**, *103* (2), 124-140; (b) Lippert, G.; Hutter, J.; Parrinello, M., A hybrid Gaussian and plane wave density functional scheme. *Mol. Phys.* **1997**, *92* (3), 477-487.
19. (a) Lee, C.; Yang, W.; Parr, R. G., Development of the Colle-Salvetti correlation-energy formula into a functional of the electron density. *Physical Review B* **1988**, *37* (2), 785-789; (b) Becke, A. D., Density-functional exchange-energy approximation with correct asymptotic behavior. *Physical Review A* **1988**, *38* (6), 3098-3100.
20. Goedecker, S.; Teter, M.; Hutter, J., Separable dual-space Gaussian pseudopotentials. *Physical Review B* **1996**, *54* (3), 1703-1710.
21. VandeVondele, J.; Hutter, J., Gaussian basis sets for accurate calculations on molecular systems in gas and condensed phases. *Journal of Chemical Physics* **2007**, *127* (11).
22. Verstraelen, T.; Van Houteghem, M.; Van Speybroeck, V.; Waroquier, M., MD-TRACKS: A Productive Solution for the Advanced Analysis of Molecular Dynamics and Monte Carlo simulations. *J Chem Inf Model* **2008**, *48* (12), 2414-2424.
23. Vandenbrande, S., Matthias Vandichel wants to thank Steven Vandenbrande for the Python script to compute the VPS spectra and the corresponding statistical errors. **2014**.

